A nanosecond pulsed electric field (nsPEF) can affect membrane permeabilization and cellular viability in a 3D spheroids tumor model

Lynn Carr, Muriel Golzio, Rosa Orlacchio, Geraldine Alberola, Jelena Kolosnjaj-Tabi, Philippe Leveque, Delia Arnaud-Cormos, Marie-Pierre Rols

Nanosecond pulsed electric field (nsPEF) can affect membrane permeabilization and cellular viability on 3D spheroids tumor model

Lynn Carr[1,2♦], Muriel Golzio[3♦], Rosa Orlacchio[1♦], Geraldine Alberola[3], Jelena Kolosnjaj-Tabi[3], Philippe Leveque[1], Delia Arnaud-Cormos[1,4*], Marie Pierre Rols[3*]

[1]Univ. Limoges, CNRS, XLIM, UMR 7252, F-87000 Limoges, France

[2] School of Electronic Engineering, Bangor University, Bangor, UK

[3] Institut de Pharmacologie et de Biologie Structurale, Université de Toulouse, CNRS, UPS, 31077, Toulouse, France

[4]Institut Universitaire de France (IUF), 75005, Paris, France

***Corresponding authors**: Marie Pierre Rols, Delia Arnaud-Cormos
Emails : Marie-Pierre.Rols@ipbs.fr , delia.arnaud-cormos@unilim.fr

♦ Contributed equally

Keywords
Electropulsation; nanosecond pulsed electric field (nsPEF); 3D cell culture; spheroids; bipolar cancellation.

Abstract

Three-dimensional (3D) cellular models represent more realistically the complexity of *in vivo* tumors compared to 2D cultures. While 3D models were largely used in classical electroporation, the effects of nanosecond pulsed electric field (nsPEF) have been poorly investigated. In this study, we evaluated the biological effects induced by nsPEF on spheroid tumor model derived from the HCT-116 human colorectal carcinoma cell line. By varying the number of pulses (from 1 to 500) and the polarity (unipolar and bipolar), the response of nsPEF exposure (10 ns duration, 50 kV/cm) was assessed either immediately after the application of the pulses or over a period lasting up to 6 days. Membrane permeabilization and cellular death occurred following the application of at least 100 pulses. The extent of the response increased with the number of pulses, with a significant decrease of viability, 24 h post-exposure, when 250 and 500 pulses were applied. The effects were highly reduced when an equivalent number of bipolar pulses were delivered. This reduction was eliminated when a 100 ns interphase interval was introduced into the bipolar pulses. Altogether, our results show that nsPEF effects, previously observed at the single cell level, also occur in more realistic 3D tumor spheroids models.

1. Introduction

Pulsed electric fields (PEFs) of microsecond duration and field strengths of 100s to 1000s V/cm are promising tools for the localized treatment of various cancers [1,2]. Plasma membrane "poration" that results from microsecond pulses is the basis of electrochemotherapy (ECT) and irreversible electroporation (IRE). During ECT, impermeable or poorly-permeable chemotherapeutics [3–5] or high doses of calcium [6,7] are introduced into the tumor cells whilst their membranes are temporarily permeabilized. IRE uses higher electric field strengths than ECT to induce permanent plasma membrane poration, which results in necrosis [8–10]. Nanosecond pulsed electric fields (nsPEF) with field strength of 10s of kV/cm can induce apoptosis or necrosis [11–13] as a result of multiple cellular effects including plasma membrane poration [12,14–16], increased intracellular calcium [12,17–20], loss of mitochondrial activity [15,21,22], and cytoskeletal disruption [15,23].

Over the last fifty years *in vitro* PEF experiments have typically been performed on cell monolayers (two-dimensional [2D] models) adhered to the bottom of flat plastic or glass cell culture plates or petri dishes. However, such models are highly simplified and fail to represent the real cellular anatomical, biochemical, and biophysical structure of tissues and organs [24,25]. In particular, the lack of the cell microenvironment cross-talk, such as cell-to-cell and cell-to-extra-cellular matrix interactions may lead to inaccurate prediction of *in vivo* situations [25–28].

Therefore, to bridge the gap between *in vitro* and *in vivo* models, three-dimensional (3D) *in vitro* models were developed to mimic the complexity of *in vivo* structures. These 3D assemblies have the advantage of being more complex than cells monolayers or cells suspensions [29]. Depending on the cell-culture technique, as well as on the specific application, numerous 3D *in vitro* models exist including organoids, cellular spheroids and organs-on-chips [30,31]. Cellular spheroids are formed by exploiting the natural tendency of certain cell types to grow and aggregate in clusters and they provide an improved 3D *in vitro* model of human solid tumors [32]. Namely, a gradient of oxygen and nutrients is established within the multicellular spheroid inducing a proliferation gradient. In the outer layers, proliferative cells are present while quiescent or dead cells can be found within the hypoxic region at the heart of the spheroid [32,33]. In addition, cell-to-cell interactions and the presence of extracellular matrix represent a microenvironment which is different from the one obtained in 2D-cultured cells (monolayers) or in cell suspensions [28]. For all these reasons, the spheroid has been shown to be an easy to use ex vivo tumor model that can reproduce or at least predict phenomena, which might occur in vivo [34].

PEF studies using spheroids have mostly investigated the effects of the pulse conditions used in ECT, typically, 8 square-wave, 100 µs duration pulses applied at 1 Hz with an electric field strength of around 1 kV/cm [35]. These parameters were shown to cause uptake of propidium iodide (PI), a marker of plasma membrane permeabilization, in both peripheral and core cells in HCT-116 spheroids up to 600 µm diameter, with peripheral cells being more intensely marked with PI [36]. This membrane permeabilization was accompanied by an absence of change in macroscopic structure over the first 24 hours and a 40% size decrease 5 days following the exposure. Plasma membrane permeabilization was confirmed in spheroids formed from other cancer cell lines (HT29, SW780, MDA6, MB231) as well as normal fibroblasts (HDF-n), which all demonstrated uptake of PI [37]. Similarly, the application of ten 5-ms pulses at 0.5 kV/cm to HCT-116 spheroids, also caused PI uptake throughout the spheroid [27].

Limited studies have investigated the effects of nsPEF on 3D cell cultures [38,39], with the aim to evaluate the occurrence of electrosensitization, i.e., the increased efficacy of nsPEF ablation when the electric pulse treatments were split in fractions [40]. Cellular spheroids of KLN205 squamous carcinoma cells exposed to a single train of 200 pulses (300 ns, 6 kV/cm at 50 Hz) resulted in 20 % cellular death whereas applying two trains of 100 pulses (300 ns, 6 kV/cm at 50 Hz), with a 100 s delay between the first and second train, resulted in 50% cellular death [38]. This electrosensitization was confirmed *in vivo* with KLN205 cells grown as subcutaneous tumors in mice [39]. This suggests that 3D cell cultures represent a valuable miniaturized tissue model providing more realistic information than 2D cell cultures.

In this study, we exposed, for the first time, cellular spheroids from the HCT-116 human colorectal carcinoma cell line to 10 ns duration pulses, with an electric field strength of 50 kV/cm, and varied pulse number and polarity. The rationale to use 10-ns electric pulses was to explore the biological outcome of very short pulses on 3D models as current literature is lacking. In addition, we aimed at comparing the biological effects obtained with 3D cells with those on 2D cell cultures of previous studies of our group. From a technical point, our generators are based on an optoelectronic technology [41,42]. Two optoelectronic photoconductive semiconductor switches are optically triggered simultaneously by a pulsed laser. 10 ns duration pulses are particularly convenient for our setup and equipment. Indeed, the pulses duration should be less than the switches charges recombination time approximately assessed between 50 and 200 ns for our components. The technology also allows us to explore pulses with shorter durations in the sub-nanosecond range for further investigations on 3D spheroids intra-cellular effects. We used live cell imaging to investigate the immediate or delayed effects on plasma membrane permeabilization, spheroid size, growth and cellular viability.

2. Material and Methods

2.1 Cell culture and spheroid formation

Human colorectal carcinoma cells HCT-116 (ATCC® CCL-247TM) stably expressing green fluorescent protein (GFP) [43] were cultured in Dulbecco's Modified Eagle Medium DMEM + 4.5 g/L of glucose (Gibco-Invitrogen, Carlsbad, USA), L-Glutamine (CSTGLU00, Eurobio, France) and pyruvate, supplemented with 10% of fetal bovine serum (F7524, Sigma, USA), and 1% of penicillin/streptomycin (P0781, Sigma, USA). Cells were kept in a humidified atmosphere at 37°C and 5% of CO_2 and were mycoplasma negative (as tested every week with MycoAlert Mycoplasma Detection kit, cat n°#LT07-318, Lonza, Switzerland). The non-adherent technique was used to generate spheroids. Briefly, 500 cells were suspended in 200 µL of culture medium and seeded in Costar® Corning® Ultra-low attachment 96 well plates (Fisher Scientific, Illkirch, France). Spheroids were kept in a humidified atmosphere at 37°C and 5% of CO_2. Cell aggregation occurred in the first 72 hours following the seeding, and allowed obtaining single spheroids of similar sizes in each well [44]. Spheroids were exposed to nsPEF after 5 days of culture when their mean diameter reached 425±5 µm and 587±7 µm (see Fig. S2 of supplementary material) for experiments presented in Fig. 6 and Fig 7, respectively. The size of the spheroids was obtained from micrographs. Precisely, the spheroids were imaged by a microscope (Incucyte® Live-Cell Imaging System). The well plates containing the spheroids (one spheroid per well) were placed in the incubator, inside which the Incucyte® microscope allows the follow-up of an individual spheroid, with the acquisition of calibrated (x,y) micrographs being obtained every hour. From these images, the spheroids diameter were measured and their area was calculated. Moreover, under all conditions, untreated spheroids were used as internal controls.

2.2 nsPEF exposure system and dosimetry

To study the effects of nsPEF on spheroids plasma membrane permeabilization, size, growth and viability, a versatile high-voltage generator was used [45]. Cells were exposed up to 500, 10 ns unipolar or bipolar pulses, with or without delay of 100 ns between the two polarities at a frequency of 20 Hz. Sham exposures were also performed under the same experimental conditions used during exposure of cells, but with the generator switched off, i.e., no nsPEF were delivered. The generator set-up and its performances are fully described in [45].

In brief, the generator is based on the frozen-wave principle [46] as shortly explained hereafter. A coaxial transmission line is used to store a bias voltage from a high-voltage DC power-supply (SR20kV-300W, Technix, France). Two optoelectronic photoconductive semiconductor switches (PCSSs) are optically triggered simultaneously by a 3-ns Nd:YAG pulsed laser (L2241A, Ekspla, Lithuania with pulse repetition rate of 20 Hz and energy up to 70 mJ per optical pulse) to allow the delivery of the electric pulses into the biological samples. Exploiting the propagation of the electromagnetic waves along the transmission line allows generating pulses of different durations. For a 10 ns duration pulse, a 2 m transmission line (RG2014 coaxial cable) is inserted between the two switches. Depending on the termination of a second switch output, either bipolar or unipolar pulses can be generated and applied to the spheroids. Specifically, when a 50 Ω charge (Barth Electronics model 2051) is connected directly to the output of the 2-port box, the wave is totally absorbed, generating unipolar pulses (Fig. 1A). If a short circuit is provided, the wave is totally reflected and its phase is inverted, resulting in a bipolar pulse (Fig. 1B). A delay between the positive and negative polarities of the bipolar pulse can be introduced by enlarging the coaxial cable between the output of the 2-port box and the second switch termination. Here, to generate bipolar (Fig. 1C) pulses with a 100 ns delay, a cable of approximately 10 m was used.

Two steel wire electrodes that are 4-mm long and 2-mm wide separated by a gap of 1.4 mm were used to deliver nsPEF to the spheroids (Fig. 2). This configuration allows for real-time observations with the microscope objective as shown in Fig. 2A.

A tap-off box (Model 245-NMFFP-100, Barth Electronics, Inc, NV, USA), connected between the generator and the electrodes, allows to measure in real-time the generated pulses, visualized on the screen of a 12 GHz oscilloscope (DSO, TDS6124C, Tektronix, USA). Pulses display on the oscilloscope show a good repeatability of their shapes. Measured pulse profiles used in the experiments are shown in Fig. 1. In all cases, for the first pulse, the maximum amplitude of the delivered voltage was approximately 7.5 kV. Peak-to-peak maximum amplitude for the bipolar pulse was approximately 14 kV. For bipolar pulses with an interphase interval of 100 ns, the maximum amplitude of the second pulse was slightly lower compared to the first pulse. The technique used to generate these pulses implies a difference in amplitude between the positive and negative polarity pulse. The amplitude decrease is mainly due to the PCSS residual resistor losses. The delayed negative polarity pulse is propagating two more times through the PCSS residual resistor. The amplitude decrease is also due to the cable losses which depend on the cable length (0.02 dB/m). Numerical simulations were performed by using the Finite Difference Time Domain (FDTD) numerical method [45]. The wire electrodes covered by a drop of pulsing medium (dielectric permittivity of 74 and conductivity of 1.4 S/m) were modeled as illustrated on Fig. 2B. The electric field distribution with a spheroid (dielectric permittivity of 40 and conductivity of 1.0 S/m) in the region between the electrodes is represented in Fig. 2C. Results show that the distributions are rather homogeneous and the electric field strength at the level of the exposed spheroid was approximately 50 kV/cm; this value is considered as a reference value for the experiments. The electric fields between the electrodes inside and outside a spheroid are shown in Fig. 2D. The electric fields inside a spheroid is slightly higher (around 60 kV/cm) due to the lowest conductivity considered in this simplified homogeneous model.

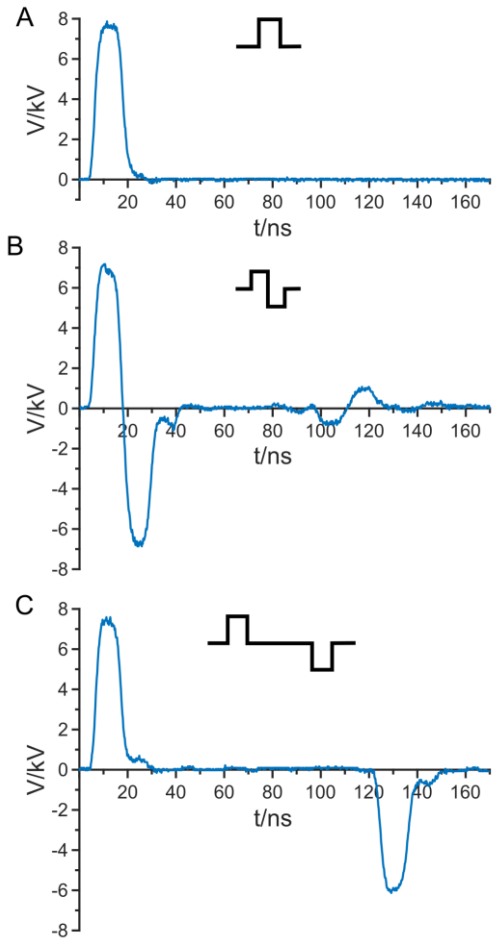

Fig. 1. Measured time-domain pulse profile for a 10-ns pulse duration: (A) unipolar, (B) bipolar and (C) bipolar with a delay of 100 ns. Voltage (V/kV) is presented as a function of time (t/ns).

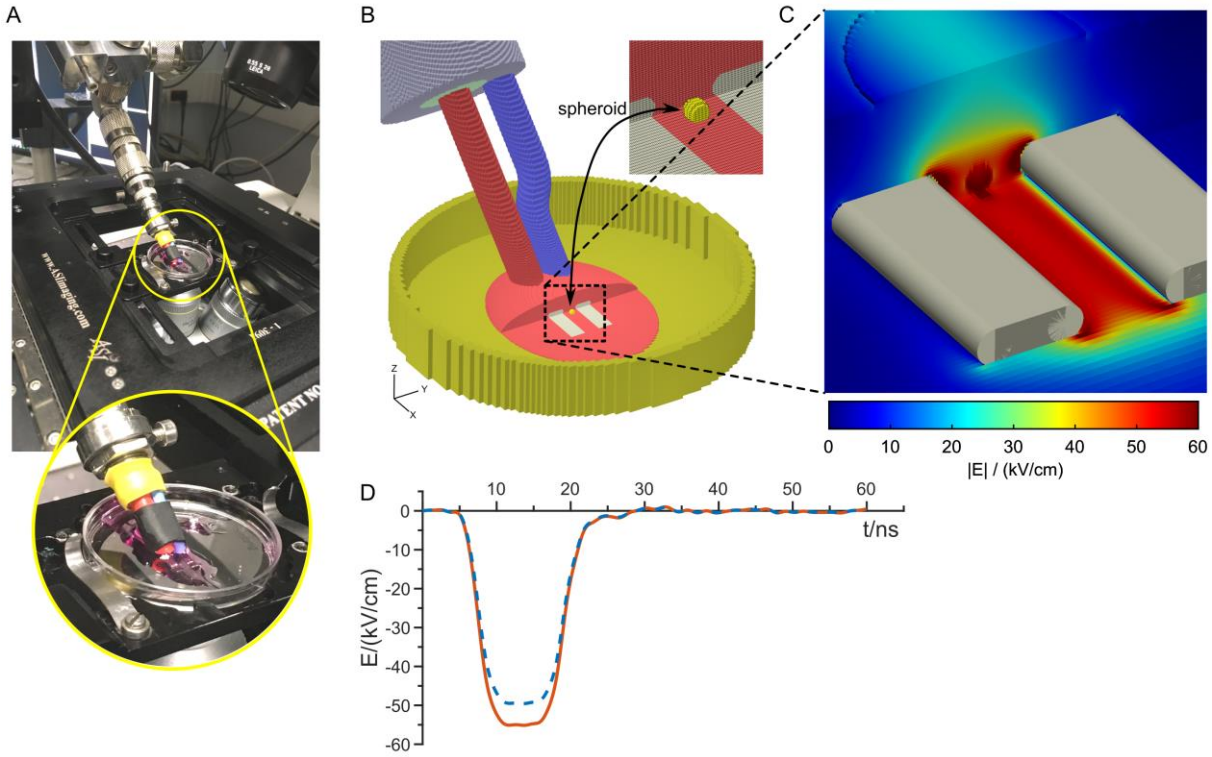

Fig. 2. Wire electrodes delivery device. A) Setup on the microscope stage, B) FDTD numerical modelling and meshing of the delivery system, the inset represent a spheroid placed between the electrodes, C) Electric field (E/(kV/cm)) distribution with a spheroid model D) Electric field (E/(kV/cm)) versus time (t/ns) between the electrodes inside (red curve) and outside (blue curve) a spheroid.

Temperature elevation of the medium during the exposure to nsPEF was measured with a fiber optic probe (Luxtron One, Lumasense Technologies, CA, USA) placed between the electrodes. In addition, microscopic temperature elevation was also retrieved from the fluorescence variation of Rhodamine-B (SigmaAldrich, Saint-Quentin Fallavier, France) using the protocol detailed in [47]. Data are in good agreement and they are shown in Fig. S1 of supplementary material.

A maximum ΔT of 7.4°C ± 0.3 °C was recorded when 500 pulses were delivered under the unipolar condition, which increased as expected with the application of bipolar pulses, either with and without delay, to 10.18 °C ± 1.26 °C. Temperature increase was induced only during the application of the electric pulses for a duration comprised between 0.5 s (10 pulses, ~0.2 °C ΔT) and 25 s (500 pulses). For viability and growth investigations, spheroids were collected from the electrodes delivery system immediately after exposure. As the experiments were performed at room temperature (22 °C), a 10 °C temperature increase would not lead to a temperature above critical physiological value. Nevertheless, electroporation can generate stresses such as thermal stress. This was demonstrated *in vivo* on a mouse model, in which the heat shock protein (HSP70) expression was monitored by the expression of a reporter gene (luciferase). Using electroporation parameters for gene transfer delivery (namely, long lasting pulses of several milliseconds), the thermal increment although moderate at the whole tissue level could be stronger inside the cells as shown by numerical 3D modeling [48]. Numerical modeling could provide additional information about this thermal increment but further experiments are needed to confirm this hypothesis as well as to characterize the cell death.

2.3 Live spheroid imaging

2.3.1. Cell permeabilization

A round 22 mm glass slide that was sandwiched into a plastic coverslip holder was placed on the microscope stage. The electrodes were lowered, using a micromanipulator, until they made contact with the glass. A spheroid was then placed between the electrodes in 500 µL of room temperature HEPES-buffered salt solution (HBSS) (NaCl 121 mM, KCl 5.4 mM, $MgCl_2$ 0.8 mM, $NaHCO_3$ 6 mM, D-glucose 5.5 mM, HEPES 25 mM and Ca^{2+} 1.8 mM, pH 7.3) containing 100 µM PI (Sigma-Aldrich #P4170).

Cells were observed by epifluorescence using a Leica DMI6000 microscope with a 10x objective. Fluorescence excitation was provided by a Spectra 7 light engine (Lumencor). Emitted light was filtered and captured on an electron-multiplying charge-coupled device camera (EMCCD Evolve 512, Roper) with 512 × 512 pixels. X-Light spinning disk (CrestOptics, Rome, Italy) was used for confocal imaging of spheroids for enhanced

fluorescence microscopy. The system was controlled by, and images were captured with, Metafluor (version 7.8 Molecular Devices). PI (excitation maximum: 493 nm; emission maximum: 636 nm) and GFP (excitation maximum: 488 nm; emission maximum: 510 nm) had an exposure time of 50 ms. Images were acquired every second for an imaging period of 240 seconds. A new spheroid was used for each experiment (n=3 to 4 spheroids).

2.3.2. Cell viability assessment

To evaluate cellular viability after exposure, each spheroid was individually placed in a well of the Costar® Corning® Ultra-low attachment 96 well plate (Fisher Scientific, Illkirch, France) containing culture medium. The plate was placed in the IncuCyte Live Cell Analysis System Microscope (Sartorius, UK) at x4 magnification (Fig. 6) and x10 magnification (Fig. 7). Spheroid growth was followed over a period of 6 days after treatment using bright field and GFP channels [49]. PI was used to assess cell viability in real-time and uptake into the spheroids was followed over a period of 48 hours following the exposure. Directly after the nsPEF exposure, culture medium containing 1 µM of PI was added into the wells. The red fluorescence due to PI penetration was followed with the IncuCyte Live Cell Analysis System Microscope with a x10 objective. Size image was 1392*1040 pixels (1.22 µm/pixel) and acquisition time was set to 400 ms and 800 ms for green and red channel, respectively. Single plane images using a wide field microscope were acquired. The focal plane was centered at the equatorial position of the spheroid. The depth of the field, which varies with numerical aperture and objective magnification, is 15.5 µm. Due to the size of the spheroid i.e. 425 µm in diameter, fluorescence signals coming from above and below are negligible.

2.4 Image processing

2.4.1. Cell permeabilization and changes in spheroid size

For permeabilization experiments image stacks from live cell imaging experiments were analyzed using Image Analyst MKII (Image Analyst Software, Novato, CA). Images were first background subtracted and a region of interest (ROI) that followed the contour of the spheroid was then drawn and relative fluorescence intensity data from the ROI was generated by Image Analyst MKII. Kymographs and line scans were created using ImageJ software [50] from a line ROI that passed from top to bottom of the spheroid. Change in spheroid size was also determined using ImageJ. The GFP images were thresholded to select the spheroid and the area was measured.

2.4.2. Cell viability

Micrographs of the green and red channels were analyzed with IncuCyte software ZOMM (Essenbio). The spheroid growth curves were evaluated from the area of the spheroid determined from green-fluorescent micrographs, plotted as a function of time every 12 h for 6 days (n=12 spheroids). The viability was determined by the PI mean fluorescence intensity from red-fluorescent micrographs and was plotted as a function of time every 6 h during 48h (n=9 spheroids). Data were exported to Microsoft excel software for the determination of the relative percentage and plotted using PRISM 5 software.

2.5. Statistical analysis

Statistical analyses were performed using Origin 2018 (OriginLab Corporation, Northampton, MA, USA) software. Datasets were first tested for normal distribution using Kolmogrov-Smirnov test. Either the non-parametric Mann-Whitney Rank or a two-way ANOVA were used. P values < 0.05, <0.01, or <0.0001 were considered statistically significant. Results are presented as mean ± SEM (Standard Error of the Mean).

3. Results and discussion

3.1 Plasma membrane permeabilization

Plasma membrane permeabilization was chosen as a primary indicator to evaluate the effect of nsPEF on spheroids. Permeabilization was assessed by following the uptake of PI, a dye that is excluded from cells with intact membranes. Uptake was visualized by confocal live cell imaging, with the optical slice going through the center of the spheroid. Uptake of PI occurred immediately after the start of nsPEF application in all exposure conditions and was still observed to occur in the minutes following pulse application (Fig. 3).

Maximal uptake of PI following unipolar exposure correlated to the number of pulses with more pulses resulting in higher uptake, the mean maximal change in fluorescence for 250 and 500 pulses being 1.6 and 2.3 times more, respectively, than that of 100 pulses. PI uptake following bipolar exposure was similarly linked to pulse number with mean maximal change in fluorescence for 250 and 500 bipolar pulses being 1.28 and 2.27 times more, respectively, than that of 100 bipolar pulses. However, unipolar pulses lead to a higher maximal uptake of PI than bipolar pulses with uptake being around three times higher when comparing the same number of pulses (mean unipolar maximal values were 2.7, 3.3 and 2.8 times higher than bipolar for 100, 250 and 500 pulses respectively). To obtain a comparable PI uptake of 100 unipolar pulses, 500 bipolar pulses have to be applied.

Note that no significant effects were elicited when the number of pulses was lower than 100.

The addition of a 100 ns delay between the phases of the bipolar pulse, for 500 pulses, resulted in an enhanced uptake of PI when compared to both 500 unipolar and bipolar pulses (maximal change in PI fluorescence in AU was 543.95±54.86, 192.62±2.79 and 669.93±94.11 respectively for unipolar, bipolar, and bipolar with 100 ns delay).

This difference between the amount of permeabilization induced by unipolar pulses and bipolar pulses, has been referred to as bipolar cancellation [51]. This phenomenon was consistently observed in numerous cell lines and for several durations of the pulse, mostly in the sub-microsecond range (from 2 to 900 ns) [52–54]. When a delay is introduced between the two phases of the bipolar pulse cancellation can still persist, but it is dependent on the duration of the delay and also the duration of the pulse [52,55,56,45]. For duration of the pulse longer than 10 ns, cancellation may occur for interphase intervals as long as 50 µs [56]. However, when a single 10 nsPEF was applied on adherent U87-MG human glioblastoma cells, at 115 kV/cm, cancellation was only observed for delays ≤ 30 ns [45]. Interphase intervals ≥ 40 ns resulted in cumulative effects, in terms of uptake of YO-PRO™-1 (YP), with the uptake observed with interphase intervals of 100 ns and 150 ns corresponding to that of two equivalent pulses of the same polarity [45]. This is consistent with the results of this study, where we show that for 500 pulses, the addition of a 100 ns delay between the phases of bipolar pulses resulted in an enhanced uptake of PI when compared to both 500 unipolar (~20% increase in fluorescence) and no delay bipolar pulses (~70% increase in fluorescence).

Why pulses of 10 ns duration maintain bipolar cancellation for only very short interphase durations could be due to an occlusion mechanism [57]. For sufficiently short intervals, the pores created by the front pulse are rapidly occluded by external molecules assisted by the back pulse, resulting in a minor uptake of PI. However, for longer interphase intervals, the occlusion phenomenon is delayed allowing for more entry of PI which results in cumulative effects similar to the application of two positive polarity pulses [45].

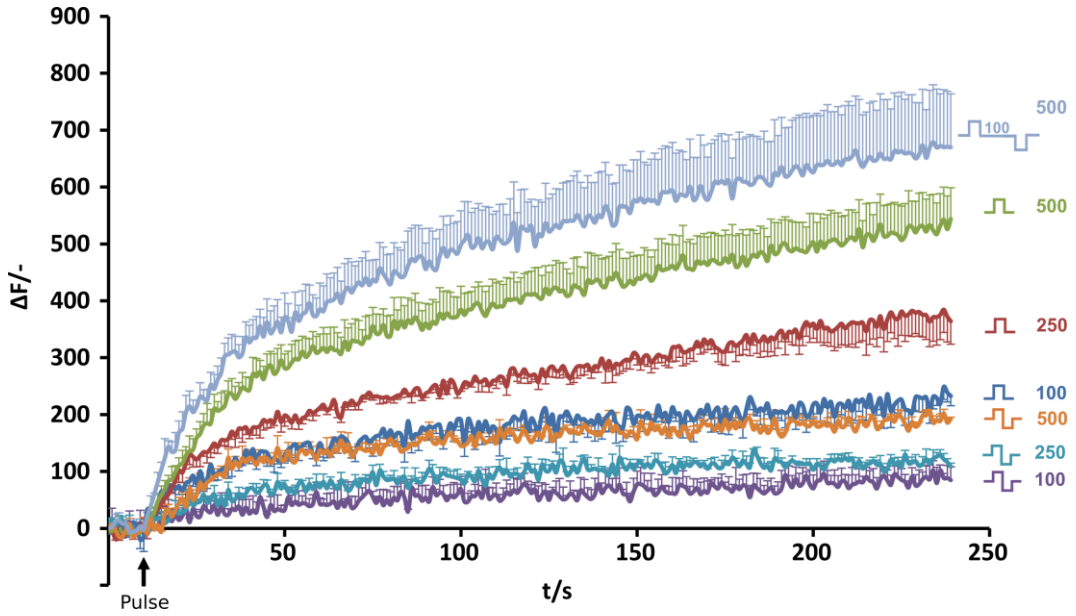

Fig. 3. Fluorescence (Δf/-) against time (t/s) plot for uptake of PI following the application of unipolar (100, 250, 500) pulses, bipolar (100, 250, 500) pulses, or 500 bipolar pulses with a 100 ns interphase delay. In all experiments 10 ns pulses were applied at 20 Hz with a 50 kV/cm electric field. Lines show average PI change over all experiments and the error bars show S.E. (n=3 for all the conditions except for 250 and 500 unipolar pulses where n=4).

The polarity of the pulse also had an effect on the spatial distribution of PI uptake (Fig. 4). Data overtime is available in the kymograph which shows intensity of fluorescence over time (left to right) and distance along ROI (top to bottom) for a line ROI that passes top to bottom along the center of the spheroid. The line scans show PI fluorescence in arbitrary units along the same line ROI at 30 seconds post-pulse and the end of the 240 second imaging period. PI at earlier times can be correlated with cell permeabilization whereas PI at 240 post pulse could be correlated with more permanent membrane alterations. In all cases, the application of 500 pulses leads to an increase in PI fluorescence throughout the whole spheroid. For unipolar exposure, there is an enhanced emission of PI in the external layer of cells proximal to the electrode at the top of the image. In the case of bipolar pulses, the fluorescence increase is fairly homogenous across the spheroid and the addition of the 100 ns interphase delay leads to more intense fluorescence in the external cells in proximity to both electrodes. Asymmetric pore formation and preferential anodal entry of YP or PI due to unipolar nsPEF were reported by several studies [55,58–61]. Anodal uptake of PI was observed in U-937 cells following the application of 10, 6 ns pulses, at 200 kV/cm.

Similar anodal YP uptake was reported in Jurkat cells exposed to 100 unipolar, 4 ns, 80 kV/cm pulses at a repetition rate of 1 kHz [60]. The anodal preference of dye uptake can be explained by differences in transmembrane potentials over the two poles of the cell [59] that may result in asymmetric distribution of the created electropores and inhomogeneous perturbation of the membrane phospholipid bilayers [58,60,62]. The homogenous uptake following bipolar exposure is in agreement with previous literature [52,60], including data obtained using µs pulse duration where similar fluorescence patterns were also observed [63]. The addition of the 100 ns interphase delay leads to more intense fluorescence in the external cells in proximity to both electrodes. We assume that the application of the back pulse determines a rapid inversion of the electrical phenomena occurring at the level of the membrane. This may result in a more homogeneous entrance of the dye throughout the spheroid, which is more pronounced when a delay is applied.

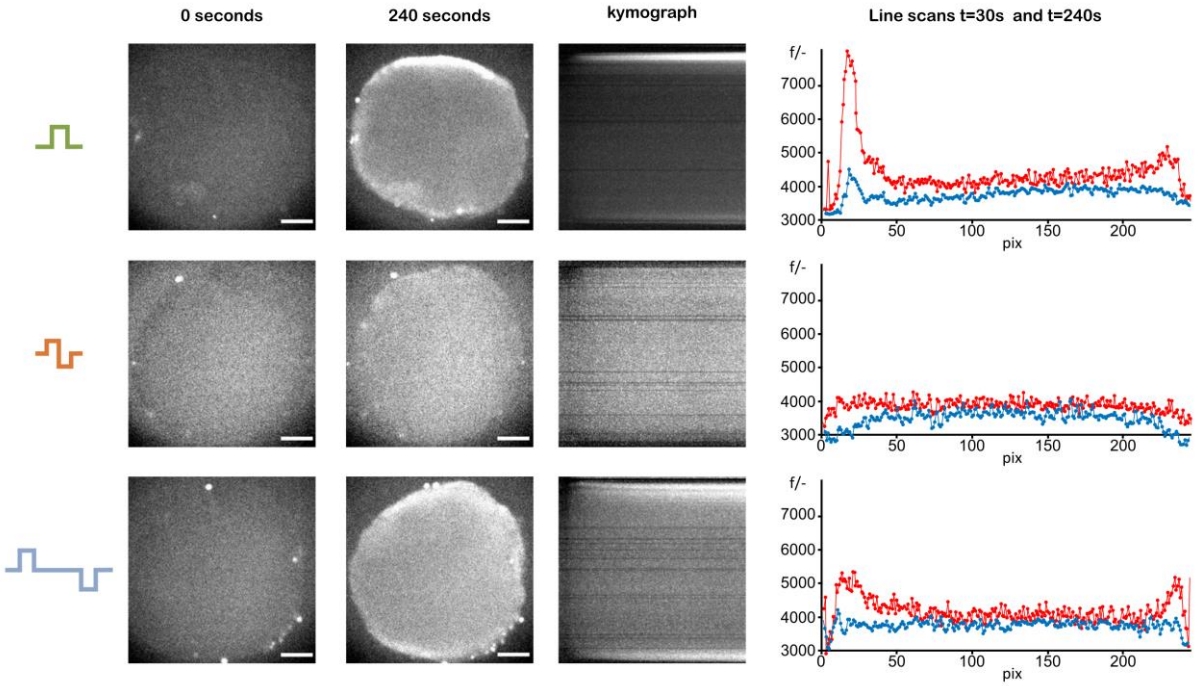

Fig. 4. Representative images of spatial distribution of PI uptake following the application of 500 unipolar, bipolar, or bipolar with 100 ns interphase delay, pulse application started at 10 seconds. The kymographs show intensity of fluorescence over time (left to right) and distance along ROI (top to bottom) for a line ROI that passes top to bottom along the center of the spheroid. The line scans show PI fluorescence in arbitrary units along the same line ROI at 30 seconds (blue) post-pulse and the end of the 240 seconds (red) imaging period. Scale bar = 50 µm.

3.2 Spheroid size

A small but rapid increase in spheroid size was also observed under all pulse conditions (Fig. 5A) with unipolar exposure resulting in a significant larger increase than an equivalent number of bipolar pulses. Compared to spheroid size before pulse, the average percentage increase in size for unipolar vs bipolar (with average % difference) was: 3.7 ± 0.4 vs 1.4 ± 0.3 (62%), 4.45 ± 0.5 vs 2.5 ± 0.1 (43%), and 3.4 ± 0.8 vs 2.5 ± 0.4 (26%), for 100, 250, and 500 pulses, respectively. The average percentage increase (62%, 43%, 26%) was dependent on the pulses number, decreasing as the pulses number increased. The addition of the 100 ns interphase delay to the 500 bipolar pulse condition resulted in an average percentage size increase (3.3 ± 0.3) comparable to that of 500 unipolar pulses (3.4 ± 0.8). The dynamics of the size increase also varied between unipolar and bipolar exposure (Fig. 5B and C) with onset of the increase occurring with the start of the pulse train for unipolar pulses and the end of the pulse train for bipolar pulses.

Such cell diameter increase was already reported during electropulsation process following µs pulse duration application and could be explained by osmotic swelling. Mammalian cells are able to maintain control over their intrinsic volume and osmotic shock causes water to accumulate in cells by osmosis. This leads first to an increase in the cell size, following which the volume decreases after the extrusion of osmolytes, through a variety of transport systems [64]. Human erythrocytes pulsed in an isotonic solution kept swelling because of continuous penetration of solutes toward equilibrium [65,66]. Swelling was also reported for CHO cells [67] and this effect could be explained by alteration of the cell cytoskeleton, due to ATP and GTP leakage during electropulsation [68]. Studies, performed on cells submitted to nsPEF, also reported swelling phenomena. Significant differences in volume regulation behavior after unipolar and bipolar nsPEF have indeed been recently published [53]. The authors showed that unipolar pulses induced cell swelling while bipolar pulses caused shrinking of human lymphoma cells in suspension. This was interpreted as differences in membrane potential recovery resulting from the different sizes of the permeabilized structures. Interestingly, not all cells have the same responses to nsPEF.

Chromaffin cells do not swell when exposed to 5 ns PEF [69]. The lack of swelling and the absence of morphology changes contrasts with cell swelling and blebbing observed for other types of cells such as Jurkat T lymphoblasts [70].

In our present study, with HCT-116 cells grown in a 3D model and submitted to nsPEF, we also observed spheroid size amplification following electropulsation, but to a significantly lower extent. Cell swelling creates a hydrodynamic influx of water, which could explain the increase in membrane permeabilization due to an increase in the size of the pores. In addition to cell swelling, transient breakdown of intercellular connections between cells in the 3D spheroid model may occur, and can also contribute to the observed change in the size of the spheroid. The exact mechanism of action and the biological consequences of exposing cells to unipolar or bipolar nsPEF have still to be determined. The understanding of the processes and causes of action related to the delay between pulses, their number and their polarity, is mandatory for determining how differences in cells and tissues responses could be further exploited both in basic research and clinical applications.

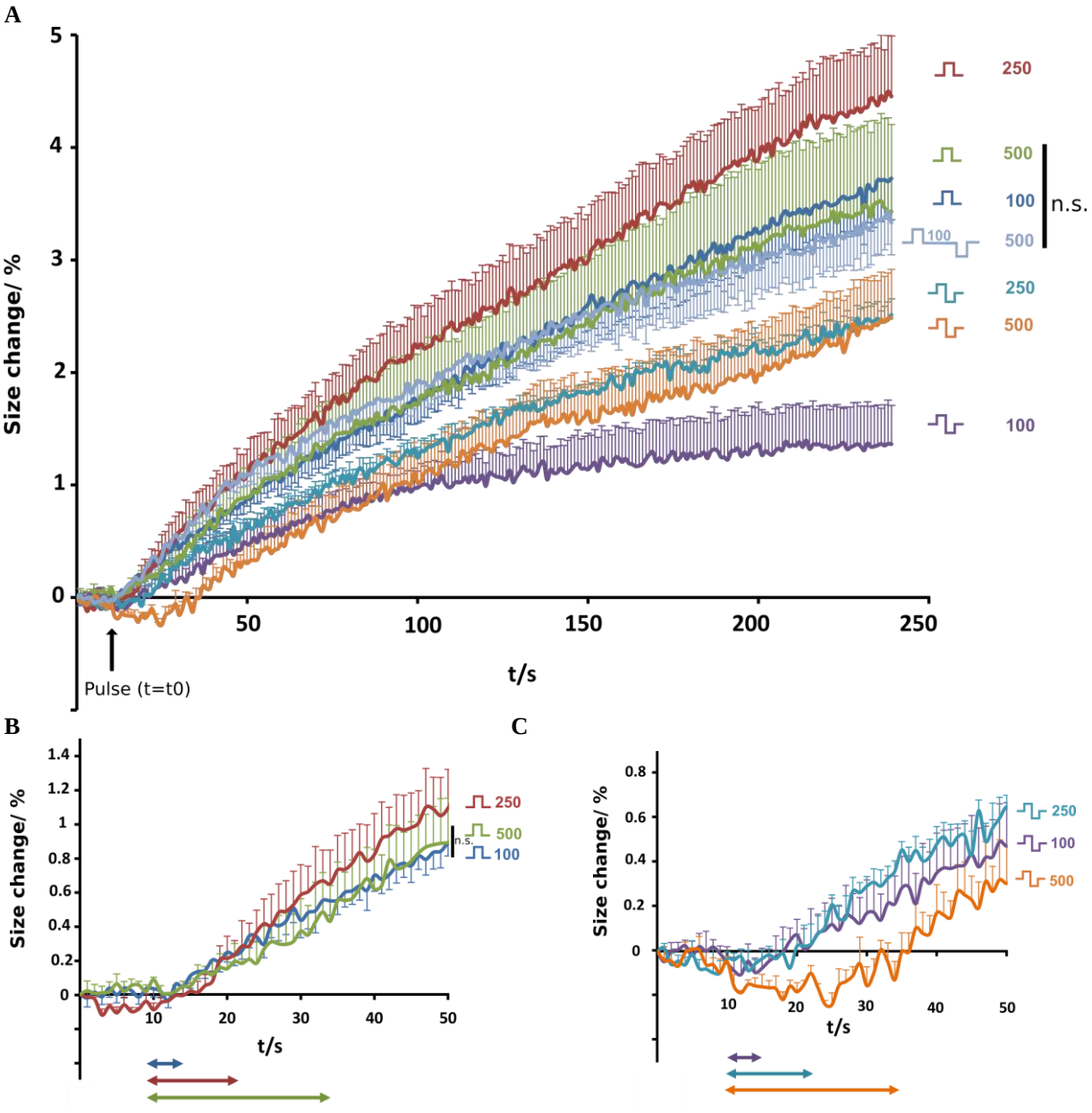

Fig. 5. A. Size change (%), over time (t/s), of spheroids compared to initial size following application of unipolar (100, 250, 500) pulses, bipolar (100, 250 and 500) pulses or 500 bipolar pulses with a 100 ns interphase delay. By focusing on the first 50 seconds of A) the onset of size increase is shown in B) for unipolar (100, 250, 500) pulses, and in C) for bipolar (100, 250 and 500) pulses. The arrows under the plots denote the duration of the pulse train (from top to bottom in both cases: 100, 250, 500 pulses). n=3 for all the conditions except for 250 and 500 unipolar pulses where n=4. All data were statistically significant except for those indicated with n.s., non-significant (Mann-Whitney test, $p < 0.05$).

3.3 Spheroid viability and growth

Live fluorescent microscopy was used to assess the longer-term impact of nsPEF exposure by observing i) the death of the cells in the spheroids 48 hours after their exposure and ii) and their ability to grow over a 6 day period. Spheroids were submitted to 1 to 500 unipolar pulses and following exposure 1 µM PI was added to the culture medium. At this point any pulse induced membrane resealing was considered to have occurred and therefore cells that were PI positive were considered non-viable. All cells in the spheroids were viable following exposure to 1, 5, or 10 pulses with no cells showing PI uptake.

100 pulses induced uptake of PI into the spheroid's peripheral cells (Fig. 6A), observed at 24 h, this effect was more pronounced following exposure to 250 pulses. Following 250 pulses, cells within the center of the spheroid were non-viable and after 500 pulses, PI uptake was observed throughout the entire spheroid. In the case of both 250 and 500 pulses breakup of the spheroid was observed, most likely due to a loss of cohesion of the structure. The mean fluorescence intensity measurements showed that PI uptake, for all conditions, occurred during the first 24 h following exposure and then plateaued (Fig. 6B).

The spheroid growth curves (GFP fluorescence area of viable cells) showed that spheroids treated with 1, 5, 10, and 50 pulses grew at a similar rate as sham exposed control spheroids. Spheroids treated with 250 pulses exhibited a slower growth rate than control and spheroids exposed to 500 pulses did not grow during the 6 days follow up (Fig. 6C). Spheroids exposed to 100 pulses exhibited a lower, but not significantly different, growth curve indicating that the cell death observed with PI during the first 24 h was not deleterious for the spheroids.

In results presented in Fig. 6A, no necrotic core within spheroids was observed compared with observations of [71], where a necrotic core on smaller spheroids was observed but only after 8 days of culture. Note that in our experiments, spheroids were exposed to nsPEF after 5 days of culture.

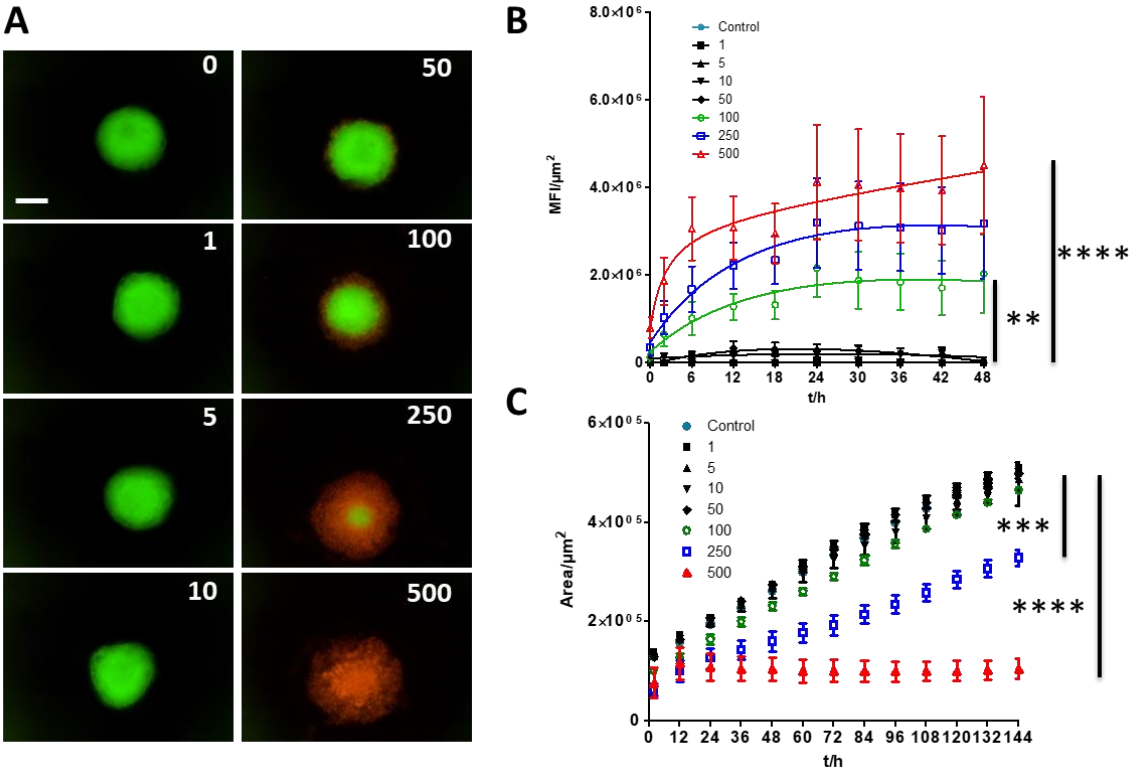

Fig. 6. Spheroid growth inhibition and cell viability depend on the number of pulses. HCT 116-GFP spheroids were treated by the application of unipolar (1, 5, 10, 50, 100, 250, 500) pulses lasting 10 ns at 20 Hz with a 50 kV/cm electric field. Subsequently, the spheroids were incubated in culture medium containing 1 µM PI during wide field fluorescence video microscopy over a period of 6 days. (A) Representative images of spheroids with Propidium iodide (PI) represented in red and GFP represented in green at 24 h. Scale: 250 µm. (B) cell viability reflected by PI uptake mean fluorescence intensities (MFI/µm²) plotted as a function of time per hour (t/h). N=2 experiments, n=9 spheroids per condition. C) Growth curves plotted from GFP fluorescence area (Area/µm²), mean ± standard error mean as a function of time per hour (t/h). N=2 experiments, n=12 spheroids per condition. Two-way ANOVA ****p < 0.0001; **p<0.01.

Long-term effect on viability and spheroid growth was then evaluated using larger spheroids of 587 µm, rather than the 425 µm used in our other experiments (Fig. 7). We found again that increasing of the number of unipolar pulses from 100 to 500, led to an increase of PI uptake (Fig. 7A and 7B). However, with these larger spheroids a yellow fluorescence in the center of spheroids was observed revealing a necrotic core [71]. The presence of the necrotic core and the spheroids initial diameter may explain the differences in cell mortality compared to results shown in Fig. 6.

We then used these larger spheroids to investigate the effect of bipolar pulses with or without an interphase delay on cell viability and spheroid growth. Following the application 100, 200 or 500 bipolar pulses, no PI labelling was observed indicating that no cell death occurred at the surface of the spheroid as for control spheroids (Fig. 7A). Quantification of the mean PI fluorescence intensities for all conditions, at various time points over 36 h showed no statistical difference in cell viability when compared to the control (Fig. 7B). Following all bipolar exposure conditions spheroid growth was also found to be comparable to control (Fig. 7C). Given that, when compared to control, the corresponding unipolar pulses resulted in decreased cell viability and decreased spheroid growth, the bipolar cancellation that was observed in Fig. 3 and 4 seems also to have a cancellation effect on these longer-term parameters. The introduction of a delay of 100 ns between the two bipolar phases resulted in a complete restauration of the unipolar effect (Fig. 7A), with no difference found in the quantification of PI fluorescence or spheroid growth when compared to the corresponding unipolar pulse (Fig. 7B and 7C).

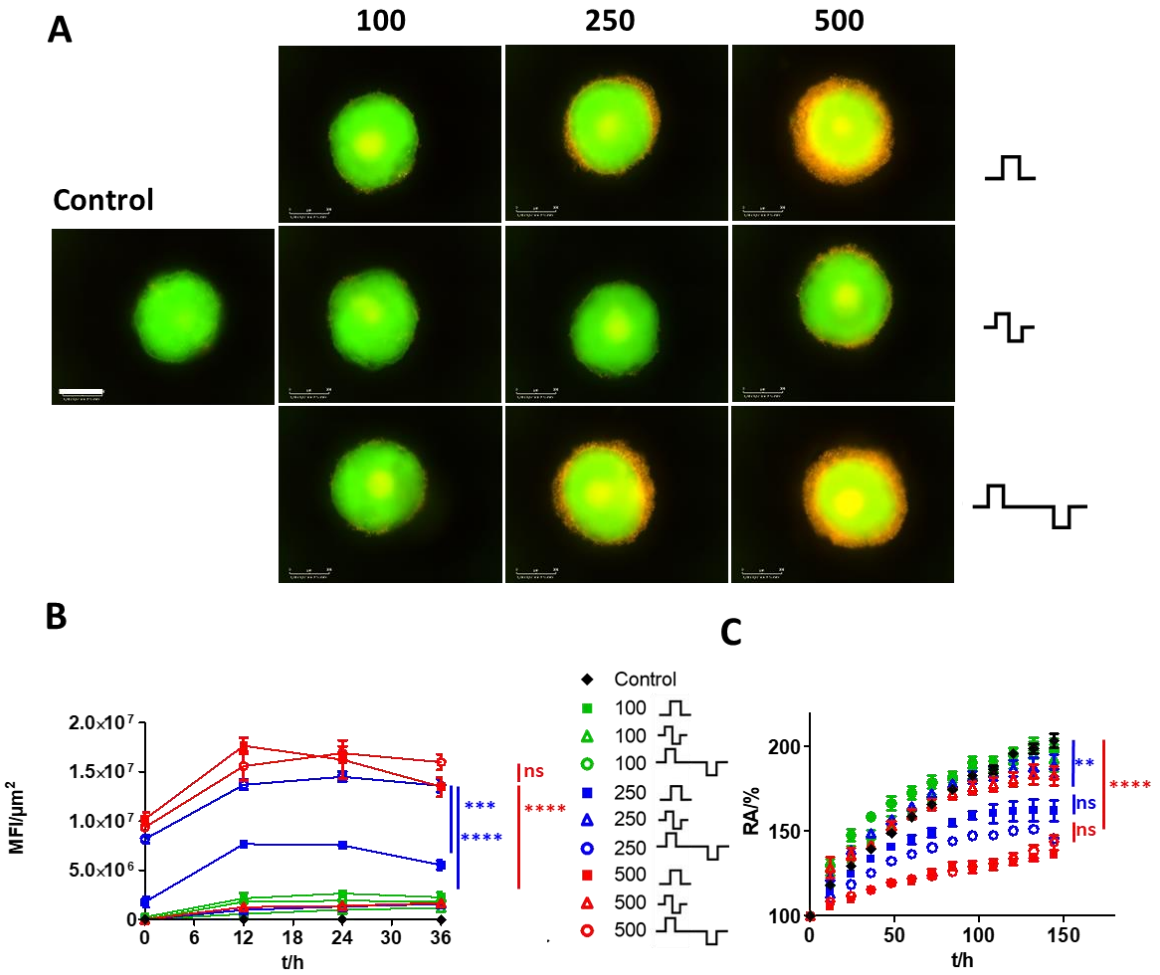

Fig. 7. Effect of bipolar pulses on cell viability and growth of spheroids. HCT 116-GFP spheroids were treated by the application of 10 ns pulses with (100, 250, 500) unipolar (uni), bipolar (bip) or bipolar pulses with 100-ns delay at 20 Hz with a 50 kV/cm electric field. Then, spheroids were incubated in culture medium containing 1 µM PI during wide field fluorescence video microscopy over a period of 6 days. (A) Representative images of spheroids with Propidium iodide (PI) in represented in red and GFP in represented in green at 24h. Scale: 300 µm. (B) cell viability reflected by PI uptake mean fluorescence intensities (MFI/µm²) plotted as a function of time per hour (t/h). N=2 experiments, n=12 spheroids per condition. (C) Growth curves extracted from GFP fluorescence area: Relative area change (RA%, mean ± standard error mean) plotted as a function of time per hour (t/h). N=2 experiments, n=12 spheroids per condition. Two-way ANOVA ****p < 0.0001; **p<0.01.

4. Conclusion

In this study, we evaluated the potential effects induced by unipolar and bipolar 10-nsPEF on cellular spheroids derived from the HCT-116 human colorectal carcinoma cell line. Different biological effects were studied including i) membrane permeabilization, ii) variation of the spheroid size, iii) cellular viability 48 h post-exposure, and iv) spheroids growth over a 6-day follow-up.

A high-voltage generator was used to provide 50 kV/cm unipolar or bipolar pulses. In addition, bipolar pulses with an interphase interval of 100 ns were also generated by modifying the delay of propagation of the electromagnetic waves.

Membrane permeabilization of the exposed spheroid was analyzed through the uptake of PI, which can only enter into cells with permeabilized membranes. As expected, by increasing the number of unipolar pulses from 100 to 500, PI uptake increased by a factor of two. Moreover, we studied the occurrence of bipolar cancellation in 3D cellular models. We demonstrated that the application of bipolar pulses with no delay between the polarities induced cancellation. PI uptake under bipolar pulses was about three times lower compared to the uptake induced by unipolar pulses, independently of the number of pulses applied. However, the addition of a 100-ns delay between the two-pulse polarities completely tapers off cancellation, resulting in additive effects with an increase of PI uptake of about 30% in comparison to unipolar pulses.

The analysis of the spatial distribution of PI uptake shows an asymmetric poration of the membrane when 500 unipolar pulses are delivered, which disappears when bipolar pulses are applied, possibly due to the switch of the electrical phenomena carried by the back pulse at the level of the cellular membrane.

The application of 100 to 500, 10-ns pulses induced a slight increase in the size of the exposed spheroids. Unipolar pulses caused a larger maximal size increase than bipolar exposure, and the size increase depending on the number of pulses.

Cellular viability of the spheroids was analyzed over a period of 48 h post-exposure. Obtained results are consistent with the observations of membrane permeabilization immediately after the pulse. Following the application of 100 pulses, permeabilization was visualized in the peripheral zone of the spheroid and increased as a function of the pulse number. The spheroids growth was also affected by the number of pulses. The application of an increased number of pulses led to a decrease of the growth of the spheroids. A complete inhibition of the spheroid growth could be achieved after application of 500 pulses, as evidenced 24 h post-exposure. Similarly, to membrane permeabilization, the application of bipolar pulses did not affect spheroids growth, suggesting that cancellation may also occur in realistic tumor models. The cancellation phenomenon was reversed by 100-ns delay between the bipolar pulses.

Our results contribute to the knowledge of the effects of short nsPEF on more realistic 3D cellular models. We have proved that cellular spheroids can be easily and efficiently used to investigate the potential effects of 10 nsPEF either monopolar or bipolar. The use of spheroids over classical 2D *in vitro* cultures appears extremely advantageous in the electroporation field because it allows obtaining important information such as membrane permeabilization or cellular viability, which are closer to the *in vivo* response, possibly avoiding or at least limiting *in vivo* experimentation. In our study, we have, for the first time, moved from 2D to 3D *in vitro* cultures in the ns duration electroporation field. We have demonstrated that some of the bioeffects observed in 2D models are confirmed in 3D cell cultures under specific exposure conditions, including membrane permeabilization, cellular swelling, or loss of cellular viability. In addition, bipolar cancellation was also observed, both as a reduction of PI uptake or inhibition of cellular growth, suggesting that this phenomenon may also occur in tissues. Further investigations would allow gaining new insights into the mechanism behind nsPEF as well as bipolar cancellation, which still remains unraveled.

Authors biographies

Lynn Carr received the B.Sc. degree (Hons) in biochemistry from University College London, London, U.K., and the master's degree in biotechnology and the Ph.D. degree from the University of Limoges, Limoges, France. As part of the XLIM Research Institute's BioEM Group, her interests focus on the effects of nanosecond pulsed electric fields on cancer cells with a particular focus on cell signaling.

Muriel Golzio was born in Montauban, France, in 1970. She received a Ph.D. in cell Biophysic from the University of Toulouse in 1999. In 2002, she join the CNRS. She is currently Director of Research in the "cellular "biophysics" team, at the IPBS-CNRS laboratory in Toulouse. Her research interests lie in the field of cell electropermeabilization (electroporation), pDNA and oligonucleotides electrotransfer and biomedical applications for Cancer treatment and Gene Therapy. She implements optical fluorescence imaging at the single cell level and in vivo by intravital multiphoton microscopy to elucidate the mechanisms of these processes.

Rosa Orlacchio was born in Sapri, Italy. She received the M.Sc. degree in Biomedical Engineering, (with honours), from "La Sapienza", University of Rome, Roma, Italy, and the Ph.D degree in Bio-electromagnetics from the Institute of Electronics and Telecommunications of Rennes (IETR), University of Rennes 1, Rennes, France, in 2014 and 2019, respectively. She is currently a Postdoctoral Researcher with the Bioelectromagnetics Team, XLIM Research Institute, CNRS, University of Limoges, Limoges, France. Her current research interests include the evaluation of the biological effects of nanosecond electric pulses on cells, and thermal electromagnetic dosimetry and microdosimetry.

Géraldine Alberola was born in France, in 1980. She received a Master of Sciences in Vectorology from the University of Toulouse in 2005. In 2005, she joined the CNRS. She is currently Engineer in the cellular biophysics team, at the IPBS-CNRS laboratory in Toulouse. Her main skills lie in skin biology and development of 3D models.

Jelena Kolosnjaj-Tabi was born in Koper, Slovenia, in 1979. She received a Master of Sciences from the Paris XI University, France, in 2006 a Master of Pharmacy in 2007 from the University of Ljubljana, Slovenia, and the Ph.D degree from Paris XI University, in 2010. She is currently a Postdoctoral Researcher with the Cellular Biophysics Team, IPBS - CNRS, Toulouse, France. Her current research interests include the biological effects of electromagnetic waves and pulsed electric fields on cells extracellular matrix (in vitro/vivo).

Philippe Leveque was born in Poitiers, France, in 1964. He received the Ph.D. degree from the University of Limoges, Limoges, France, in 1994. In 1995, he joined C.N.R.S. He is involved in the development of dosimetry and exposure setups for health-risk assessment in cooperation with biological and medical research groups. He is currently a Senior Scientist with CNRS and the Group Leader of Bioelectromagnetics Team with the XLIM Research Institute focusing on nanopulse application. His current research interest includes the scattering problems of electromagnetic waves, particularly in the time domain.

Delia Arnaud-Cormos was born in Cugir, Romania, in 1978. She received the Ph.D. degree from INSA Rennes, France, in 2006. Since 2007, she is an Associate Professor with the Bioelectromagnetics Team, XLIM Institute, University of Limoges/CNRS, Limoges, France. In 2012, she joined the University of Southern California, Los Angeles, USA, where she developed research with the Pulsed Power Group. Since 2018, she has been a Junior Member with the Institut Universitaire de France, Paris, France, and a member of the International Bioelectrics Consortium. Her current research interests include nanosecond pulses/microwave exposure system setup and dosimetric characterization for bioelectromagnetic studies.

Marie-Pierre Rols was born in Decazeville, France, in 1962. She received a Ph.D. in Cell Biophysics from the University of Toulouse in 1989. In 1990, she joined the CNRS. She is currently Director of Research at the IPBS-CNRS laboratory in Toulouse, Group Leader of the "cellular biophysics" team and head of the "Structural Biology and Biophysics" Department. She belongs to the council of the ISEBTT and BES societies and of the Bioelectrics Consortium. Her research interests lie in the fields of membrane electropermeabilization in cells and tissues from the basics to the development of applications.

Authors contributions:

Experiments and the study were designed by MPR, MG, DAC and PL. RO, DAC and PL designed, conceived the generator and numerical modeling. MG, LC, MPR, GA, JKT contributed to the acquisition and analysis of biological data. All authors contributed to analysis and interpretation of data and drafting the manuscript. All authors read and gave approval of the final version to be submitted.

Acknowledgements

This work was supported by the Canceropole Grand Sud-Ouest [grant number 2018-EC26], GDR 2025 HAPPYBIO, Region Nouvelle-Aquitaine [grant number AAPR2020A- 2019-8152210] and European Union's Horizon 2020 research and innovation program under grant agreement No 737164.

References

[1] J. Kolosnjaj-Tabi, L. Gibot, I. Fourquaux, M. Golzio, M.-P. Rols, Electric field-responsive nanoparticles and electric fields: physical, chemical, biological mechanisms and therapeutic prospects, Adv. Drug Deliv. Rev. 138 (2019) 56–67. https://doi.org/10.1016/j.addr.2018.10.017.

[2] R. Nuccitelli, Application of pulsed electric fields to cancer therapy, Bioelectricity. 1 (2019) 30–34. https://doi.org/10.1089/bioe.2018.0001.

[3] L.M. Mir, J. Gehl, G. Sersa, C.G. Collins, J.-R. Garbay, V. Billard, P.F. Geertsen, Z. Rudolf, G.C.O. Sullivan, M. Marty, Standard operating procedures of the electrochemotherapy : Instructions for the use of bleomycin or cisplatin administered either systemically or locally and electric pulses delivered by the Cliniporator TM by means of invasive or non-invasive electrodes, EJC Suppl. 4 (2006) 14–25. https://doi.org/10.1016/j.ejcsup.2006.08.003.

[4] D. Miklavčič, G. Sersa, E. Brecelj, J. Gehl, D. Soden, G. Bianchi, P. Ruggieri, C.R. Rossi, L.G. Campana, T. Jarm, Electrochemotherapy : technological advancements for efficient electroporation-based treatment of internal tumors, Med. Biol. Eng. Comput. 50 (2012) 1213–1225. https://doi.org/10.1007/s11517-012-0991-8.

[5] S. Orlowski, J. Belehradek, C. Paoletti, L.M. Mir, Transient electropermeabilization of cells in culture. Increase of the cytotoxicity of anticancer drugs, Biochem. Pharmacol. 37 (1988) 4727–4733. https://doi.org/10.1016/0006-2952(88)90344-9.

[6] H. Falk, L.W. Matthiessen, G. Wooler, J. Gehl, Calcium electroporation for treatment of cutaneous metastases ; a randomized double- blinded phase II study , comparing the effect of calcium electroporation with electrochemotherapy, Acta Oncol. 0 (2017) 1–9. https://doi.org/10.1080/0284186X.2017.1355109.

[7] S.K. Frandsen, H. Gissel, P. Hojman, T. Tramm, J. Eriksen, J. Gehl, Direct therapeutic applications of calcium electroporation to effectively induce tumor necrosis, Cancer Res. 72 (2012) 1336–1341. https://doi.org/10.1158/0008-5472.CAN-11-3782.

[8] R.V. Davalos, I.L.M. Mir, B. Rubinsky, Tissue ablation with irreversible electroporation, Ann. Biomed. Eng. 33 (2005) 223–231. https://doi.org/10.1007/s10439-005-8981-8.

[9] L. Miller, J. Leor, B. Rubinsky, Cancer cells ablation with irreversible electroporation, Technol. Cancer Res. Treat. 4 (2005) 699–705. https://doi.org/10.1177/153303460500400615.

[10] C. Jiang, R.V. Davalos, J.C. Bischof, A review of basic to clinical studies of irreversible electroporation therapy, IEEE Trans. Biomed. Eng. 62 (2015) 4–20. https://doi.org/10.1109/TBME.2014.2367543.

[11] S.J. Beebe, P.M. Fox, L.J. Rec, K. Somers, R.H. Stark, K.H. Schoenbach, Nanosecond pulsed electric field (nsPEF) effects on cells and tissues: apoptosis induction and tumor growth inhibition, IEEE Trans. Plasma Sci. 30 (2002) 286–292. https://doi.org/10.1109/TPS.2002.1003872.

[12] S.J. Beebe, J. White, P.F. Blackmore, Y. Deng, K. Somers, K.H. Schoenbach, Diverse effects of nanosecond pulsed electric fields on cells and tissues., DNA Cell Biol. 22 (2003) 785–96. https://doi.org/10.1089/104454903322624993.

[13] S.J. Beebe, P.M. Fox, L.J. Rec, L.K. Willis, K.H. Schoenbach, Nanosecond, high-intensity pulsed electric fields induce apoptosis in human cells., FASEB J. Off. Publ. Fed. Am. Soc. Exp. Biol. 17 (2003) 1493–5. https://doi.org/10.1096/fj.02-0859fje.

[14] A.M. Bowman, O.M. Nesin, O.N. Pakhomova, A.G. Pakhomov, Analysis of plasma membrane integrity by fluorescent detection of Tl(+) uptake., J. Membr. Biol. 236 (2010) 15–26. https://doi.org/10.1007/s00232-010-9269-y.

[15] L. Carr, S.M. Bardet, R.C. Burke, D. Arnaud-Cormos, P. Leveque, R.P.O. Connor, Calcium-independent disruption of microtubule dynamics by nanosecond pulsed electric fields in U87 human glioblastoma cells, Sci. Rep. 7 (2017) 41267. https://doi.org/10.1038/srep41267.

[16] E.B. Sözer, Y.-H. Wu, S. Romeo, P.T. Vernier, Nanometer-scale permeabilization and osmotic swelling induced by 5-ns pulsed electric fields, J. Membr. Biol. 250 (2017) 21–30. https://doi.org/10.1007/s00232-016-9918-x.
[17] P.T. Vernier, Y. Sun, L. Marcu, S. Salemi, C.M. Craft, M.A. Gundersen, Calcium bursts induced by nanosecond electric pulses, Biochem. Biophys. Res. Commun. 310 (2003) 286–295. https://doi.org/10.1016/j.bbrc.2003.08.140.
[18] J.A. White, P.F. Blackmore, K.H. Schoenbach, S.J. Beebe, Stimulation of capacitative calcium entry in HL-60 cells by nanosecond pulsed electric fields., J. Biol. Chem. 279 (2004) 22964–72. https://doi.org/10.1074/jbc.M311135200.
[19] L. Carr, S.M. Bardet, D. Arnaud-Cormos, P. Leveque, R.P.O. Connor, Visualisation of an nsPEF induced calcium wave using the genetically encoded calcium indicator GCaMP in U87 human glioblastoma cells, Bioelectrochemistry. 119 (2018) 68–75. https://doi.org/10.1016/j.bioelechem.2017.09.003.
[20] I. Semenov, S. Xiao, A.G. Pakhomov, Primary pathways of intracellular Ca(2+) mobilization by nanosecond pulsed electric field., Biochim. Biophys. Acta. 1828 (2013) 981–9. https://doi.org/10.1016/j.bbamem.2012.11.032.
[21] T.B. Napotnik, Y.-H. Wu, M.A. Gundersen, D. Miklavčič, P.T. Vernier, Nanosecond electric pulses cause mitochondrial membrane permeabilization in Jurkat cells., Bioelectromagnetics. 33 (2012) 257–64. https://doi.org/10.1002/bem.20707.
[22] S.J. Beebe, Y.-J. Chen, N.M. Sain, K.H. Schoenbach, S. Xiao, Transient features in nanosecond pulsed electric fields differentially modulate mitochondria and viability., PloS One. 7 (2012) e51349. https://doi.org/10.1371/journal.pone.0051349.
[23] G.L. Thompson, C.C. Roth, D.R. Dalzell, M. Kulpers, B.L. Ibey, Calcium influx affects intracellular transport and membrane repair following nanosecond pulsed electric field exposure, J. Biomed. Opt. 19 (2014) 055005.
[24] G. Huang, F. Li, X. Zhao, Y. Ma, Y. Li, M. Lin, G. Jin, T.J. Lu, G.M. Genin, F. Xu, Functional and biomimetic materials for engineering of the three-dimensional cell microenvironment, Chem. Rev. 117 (2017) 12764–12850. https://doi.org/10.1021/acs.chemrev.7b00094.
[25] F. Pampaloni, E.G. Reynaud, E.H.K. Stelzer, The third dimension bridges the gap between cell culture and live tissue, 8 (2007) 839–845.
[26] A. Nyga, U. Cheema, M. Loizidou, 3D tumour models : novel in vitro approaches to cancer studies, J. Cell Commun. Signal. 5 (2011) 239–248. https://doi.org/10.1007/s12079-011-0132-4.
[27] L. Wasungu, J. Escoffre, A. Valette, J. Teissie, M. Rols, A 3D in vitro spheroid model as a way to study the mechanisms of electroporation, Int. J. Pharm. 379 (2009) 278–284. https://doi.org/10.1016/j.ijpharm.2009.03.035.
[28] S. Nath, G.R. Devi, Three-dimensional culture systems in cancer research: Focus on tumor spheroid model, Pharmacol. Ther. 163 (2016) 94–108. https://doi.org/10.1016/j.pharmthera.2016.03.013.
[29] R.M. Sutherland, Cell and environment interactions in tumor microregions: the multicell spheroid model, Science. 240 (1988) 177–184.
[30] C. Jensen, Y. Teng, Is It time to start transitioning from 2D to 3D cell culture?, Front. Mol. Biosci. 7 (2020) 33. https://doi.org/10.3389/fmolb.2020.00033.
[31] Z. Koledova, ed., 3D cell culture: methods and protocols, Humana Press, 2017. https://doi.org/10.1007/978-1-4939-7021-6.
[32] A.S. Nunes, I.J. Correia, E.C. Costa, 3D tumor spheroids as in vitro models to mimic in vivo human solid tumors resistance to therapeutic drugs, Biotechnol. Bioeng. 116 (2019) 206–226. https://doi.org/10.1002/bit.26845.
[33] J. Friedrich, R. Ebner, L.A. Kunz-Schughart, Experimental anti-tumor therapy in 3-D: spheroids--old hat or new challenge?, Int. J. Radiat. Biol. 83 (2007) 849–871.
[34] H.R. Mellor, L.A. Davies, H. Caspar, C.R. Pringle, S.C. Hyde, D.R. Gill, R. Callaghan, Optimising non-viral gene delivery in a tumour spheroid model, J. Gene Med. 8 (2006) 1160–1170.
[35] M. Marty, G. Sersa, J.R. Garbay, J. Gehl, C.G. Collins, M. Snoj, V. Billard, P.F. Geertsen, J.O. Larkin, D. Miklavcic, I. Pavlovic, S.M. Paulin-Kosir, M. Cemazar, N. Morsli, D.M. Soden, Z. Rudolf, C. Robert, G.C.O. Sullivan, L.M. Mir, Electrochemotherapy – An easy , highly effective and safe treatment of cutaneous and subcutaneous metastases : Results of ESOPE (European Standard Operating Procedures of Electrochemotherapy) study, EJC Suppl. 4 (2006) 3–13. https://doi.org/10.1016/j.ejcsup.2006.08.002.
[36] L. Gibot, L. Wasungu, J. Teissié, M. Rols, Antitumor drug delivery in multicellular spheroids by electropermeabilization ☆, J. Controlled Release. 167 (2013) 138–147. https://doi.org/10.1016/j.jconrel.2013.01.021.
[37] S.K. Frandsen, L. Gibot, M. Madi, J. Gehl, M.-P. Rols, Calcium electroporation: Evidence for differential effects in normal and malignant cell lines, evaluated in a 3D spheroid model, PLOS ONE. 10 (2015) e0144028. https://doi.org/10.1371/journal.pone.0144028.

[38] C. Muratori, A.G. Pakhomov, S. Xiao, O.N. Pakhomova, Electrosensitization assists cell ablation by nanosecond pulsed electric field in 3D cultures, Sci. Rep. 6 (2016) 23225. https://doi.org/10.1038/srep23225.
[39] C. Muratori, A.G. Pakhomov, L. Heller, M. Casciola, E. Gianulis, S. Grigoryev, S. Xiao, O.N. Pakhomova, Electrosensitization increases antitumor effectiveness of nanosecond pulsed electric fields in vivo, Technol. Cancer Res. Treat. 16 (2017) 987–996. https://doi.org/10.1177/1533034617712397.
[40] O.N. Pakhomova, B.W. Gregory, V.A. Khorokhorina, A.M. Bowman, S. Xiao, A.G. Pakhomov, Electroporation-induced electrosensitization, PLoS ONE. 6 (2011). https://doi.org/10.1371/journal.pone.0017100.
[41] S. El Amari, A. De Angelis, D. Arnaud-Cormos, V. Couderc, P. Leveque, Characterization of a linear photoconductive switch used in nanosecond pulsed electric field generator, IEEE Photonics Technol. Lett. 23 (2011) 673–675.
[42] S. Kohler, V. Couderc, R.P. O'Connor, D. Arnaud-Cormos, P. Leveque, A versatile high voltage nano- and sub-nanosecond pulse generator, IEEE Trans. Dielectr. Electr. Insul. 20 (2013) 1201–1208.
[43] S. Pelofy, J. Teissié, M. Golzio, S. Chabot, Chemically modified oligonucleotide-increased stability negatively correlates with its efficacy despite efficient electrotransfer, J. Membr. Biol. 245 (2012) 565–571. https://doi.org/10.1007/s00232-012-9468-9.
[44] L. Gibot, J. Kolosnjaj-Tabi, E. Bellard, T. Chretiennot, Q. Saurin, A. Catrain, M. Golzio, R. Vézinet, M.-P. Rols, Evaluations of acute and sub-acute biological effects of narrowband and moderate-band high power electromagnetic waves on cellular spheroids, Sci. Rep. 9 (2019) 15324. https://doi.org/10.1038/s41598-019-51686-9.
[45] R. Orlacchio, L. Carr, C. Palego, D. Arnaud-Cormos, P. Leveque, High-voltage 10 ns delayed paired or bipolar pulses for in vitro bioelectric experiments, Bioelectrochemistry. 137 (2021) 107648.
[46] D. Arnaud-Cormos, V. Couderc, P. Leveque, Photoconductive switching for pulsed high-voltage generators, in: D. Miklavcic (Ed.), Handb. Electroporation, Springer International Publishing, Cham, 2017: pp. 1–21. https://doi.org/10.1007/978-3-319-26779-1_208-1.
[47] A. Nefzi, L. Carr, C. Dalmay, A. Pothier, P. Leveque, D. Arnaud-Cormos, Microdosimetry using Rhodamine B within macro- and microsystems for radiofrequency signals exposures of biological samples, IEEE Trans. Microw. Theory Tech. (2019) 1–9.
[48] T. Forjanic, B. Markelc, M. Marcan, E. Bellard, F. Couillaud, M. Golzio, D. Miklavci, Electroporation-induced stress response and its effect on gene electrotransfer efficacy: in vivo imaging and numerical modeling, IEEE Trans. Biomed. Eng. 66 (2019) 2671–2683.
[49] E. Griseti, N. Merbahi, M. Golzio, Anti-cancer potential of two plasma-activated liquids: implication of long-lived reactive oxygen and nitrogen species, Cancers. 12 (2020). https://doi.org/10.3390/cancers12030721.
[50] C.A. Schneider, W.S. Rasband, K.W. Eliceiri, NIH Image to ImageJ : 25 years of image analysis, Nat. Methods. 9 (2012) 671–675. https://doi.org/10.1038/nmeth.2089.
[51] A.G. Pakhomov, I. Semenov, S. Xiao, O.N. Pakhomova, B. Gregory, K.H. Schoenbach, J.C. Ullery, H.T. Beier, S.R. Rajulapati, B.L. Ibey, Cancellation of cellular responses to nanoelectroporation by reversing the stimulus polarity, Cell. Mol. Life Sci. CMLS. 71 (2014) 4431–4441. https://doi.org/10.1007/s00018-014-1626-z.
[52] C.M. Valdez, R. Barnes, C.C. Roth, E. Moen, B. Ibey, The interphase interval within a bipolar nanosecond electric pulse modulates bipolar cancellation, Bioelectromagnetics. 39 (2018) 441–450. https://doi.org/10.1002/bem.22134.
[53] E.B. Sözer, P.T. Vernier, Modulation of biological responses to 2 ns electrical stimuli by field reversal, Biochim. Biophys. Acta BBA - Biomembr. 1861 (2019) 1228–1239.
[54] M. Casciola, S. Xiao, F. Apollonio, A. Paffi, M. Liberti, C. Muratori, A.G. Pakhomov, Cancellation of nerve excitation by the reversal of nanosecond stimulus polarity and its relevance to the gating time of sodium channels, Cell. Mol. Life Sci. 76 (2019) 4539–4550. https://doi.org/10.1007/s00018-019-03126-0.
[55] C.M. Valdez, R.A. Barnes, C.C. Roth, E.K. Moen, G.A. Throckmorton, B.L. Ibey, Asymmetrical bipolar nanosecond electric pulse widths modify bipolar cancellation, Sci. Rep. 7 (2017). https://doi.org/10.1038/s41598-017-16142-6.
[56] E.C. Gianulis, M. Casciola, S. Xiao, O.N. Pakhomova, A.G. Pakhomov, Electropermeabilization by uni- or bipolar nanosecond electric pulses: The impact of extracellular conductivity, Bioelectrochemistry. 119 (2018) 10–19. https://doi.org/10.1016/j.bioelechem.2017.08.005.
[57] T.R. Gowrishankar, J.V. Stern, K.C. Smith, J.C. Weaver, Nanopore occlusion: A biophysical mechanism for bipolar cancellation in cell membranes, Biochem. Biophys. Res. Commun. 503 (2018) 1194–1199. https://doi.org/10.1016/j.bbrc.2018.07.024.

[58] E.B. Sözer, C.F. Pocetti, P.T. Vernier, Asymmetric patterns of small molecule transport after nanosecond and microsecond electropermeabilization, J. Membr. Biol. 251 (2018) 197–210. https://doi.org/10.1007/s00232-017-9962-1.
[59] W. Frey, J.A. White, R.O. Price, P.F. Blackmore, R.P. Joshi, R. Nuccitelli, S.J. Beebe, K.H. Schoenbach, J.F. Kolb, Plasma membrane voltage changes during nanosecond pulsed electric field exposure, Biophys. J. 90 (2006) 3608–3615. https://doi.org/10.1529/biophysj.105.072777.
[60] P.T. Vernier, Y. Sun, M.A. Gundersen, Nanoelectropulse-driven membrane perturbation and small molecule permeabilization, BMC Cell Biol. 7 (2006) 37. https://doi.org/10.1186/1471-2121-7-37.
[61] W. Bo, M. Silkunas, U. Mangalanathan, V. Novickij, M. Casciola, I. Semenov, S. Xiao, O.N. Pakhomova, A.G. Pakhomov, Probing nanoelectroporation and resealing of the cell membrane by the entry of Ca2+ and Ba2+ ions, Int. J. Mol. Sci. 21 (2020). https://doi.org/10.3390/ijms21093386.
[62] P.T. Vernier, Y. Sun, L. Marcu, C.M. Craft, M.A. Gundersen, Nanosecond pulsed electric fields perturb membrane phospholipids in T lymphoblasts, FEBS Lett. 572 (2004) 103–108. https://doi.org/10.1016/j.febslet.2004.07.021.
[63] C. Faurie, E. Phez, M. Golzio, C. Vossen, J.-C. Lesbordes, C. Delteil, J. Teissié, M.-P. Rols, Effect of electric field vectoriality on electrically mediated gene delivery in mammalian cells, Biochim. Biophys. Acta BBA - Biomembr. 1665 (2004) 92–100. https://doi.org/10.1016/j.bbamem.2004.06.018.
[64] N. Mccarty, R. O'neil, Calcium signaling in cell volume regulation., Physiol. Rev. (1992). https://doi.org/10.1152/PHYSREV.1992.72.4.1037.
[65] K. Kinosita, T.Y. Tsong, Voltage-induced pore formation and hemolysis of human erythrocytes, Biochim. Biophys. Acta BBA - Biomembr. 471 (1977) 227–242. https://doi.org/10.1016/0005-2736(77)90252-8.
[66] K. Kinosita, T.Y. Tsong, Formation and resealing of pores of controlled sizes in human erythrocyte membrane, Nature. 268 (1977) 438–441. https://doi.org/10.1038/268438a0.
[67] M. Golzio, M.P. Mora, C. Raynaud, C. Delteil, J. Teissié, M.P. Rols, Control by osmotic pressure of voltage-induced permeabilization and gene transfer in mammalian cells, Biophys. J. 74 (1998) 3015–3022. https://doi.org/10.1016/S0006-3495(98)78009-9.
[68] M.P. Rols, J. Teissié, Electropermeabilization of mammalian cells to macromolecules: control by pulse duration., Biophys. J. 75 (1998) 1415–1423.
[69] G.L. Craviso, C. Fisher, I. Chatterjee, P. Thomas Vernier, Adrenal chromaffin cells do not swell when exposed to nanosecond electric pulses, Bioelectrochemistry. 103 (2015) 98–102. https://doi.org/10.1016/j.bioelechem.2014.08.006.
[70] S. Romeo, Y.-H. Wu, Z.A. Levine, M.A. Gundersen, P.T. Vernier, Water influx and cell swelling after nanosecond electropermeabilization, Biochim. Biophys. Acta BBA - Biomembr. 1828 (2013) 1715–1722. https://doi.org/10.1016/j.bbamem.2013.03.007.
[71] E. Griseti, J. Kolosnjaj-Tabi, L. Gibot, I. Fourquaux, M.-P. Rols, M. Yousfi, N. Merbahi, M. Golzio, Pulsed electric field treatment enhances the cytotoxicity of plasma-activated lquids in a three-dimensional human colorectal cancer cell model, Sci. Rep. 9 (2019) 7583. https://doi.org/10.1038/s41598-019-44087-5.